Electronic Supplementary Material (ESI) for Nanoscale.
This journal is © The Royal Society of Chemistry 2020

Supporting Information

The Recovery of nano-sized carbon black filler structure and its contribution to the stress recovery in rubber nanocomposites

Liang Chen[1#], Lihui Wu[1#], Lixian Song[2], Zhijie Xia[1], Yuanfei Lin[1, 3], Wei Chen[1*],

Liangbin Li[1]

1. National Synchrotron Radiation Lab and CAS Key Laboratory of Soft Matter Chemistry, Anhui Provincial Engineering Laboratory of Advanced Functional Polymer Film, University of Science and Technology of China, Hefei, 230029, China

2. State Key Laboratory of Environment-friendly Energy Materials, Southwest University of Science and Technology, Mianyang, 621010, China

3. South China Advanced Institute for Soft Matter Science and Technology, South China University of Technology, Guangzhou, 510640, China

Corresponding author, E-mail: wc003@ustc.edu.cn

1. The 2D Images Collecting and 3D Constructing by X-ray Nano-CT

Figure S1 is the schematic view of X-ray Nano-CT. The monochromatic X-rays from Synchrotron Radiation are first focused by a Capillary condenser. After transmitting through the samples, the X-rays are then collected by a micro zone plate, and then detected by X-ray CCD and the 2D projections were obtained. During 3D imaging, the samples were installed on a rotation stage. Each time the tilting angle is 0.5° and then the series of projections were obtained. The projections were then reconstructed into 3D Imaging and again cut into series of slices for further segmenting, dying and quantitatively analyzing.

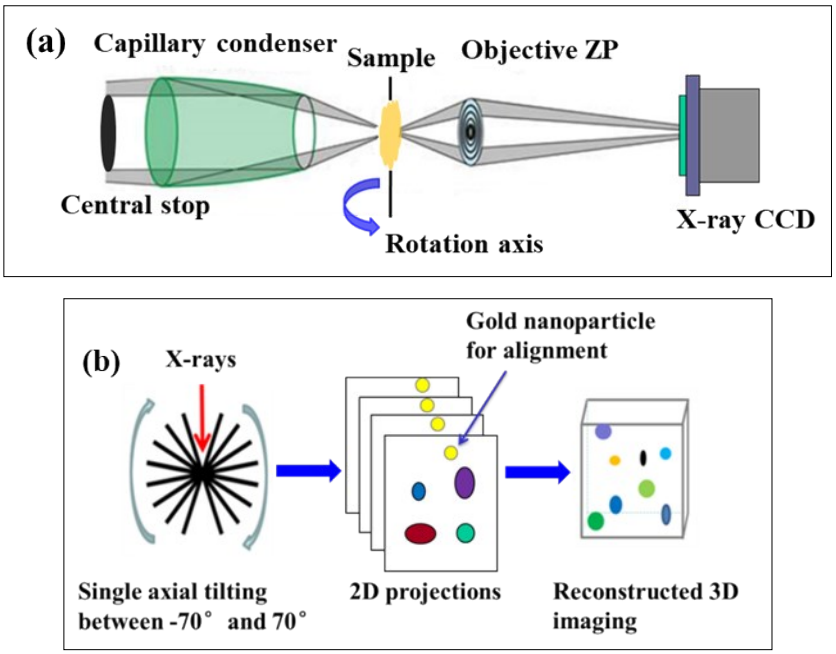

Figure S1. (a) The schematic of X-ray 2D projections acquiring and (b) the method of 3D imaging reconstructing.

2. The Payne Effects of Filled Rubber Used in The Experiment

The Payne effects of the experimental samples were measured on a stress

controlled rheometer (AR-G2, TA Instruments, US) with a plate geometry (diameter 20 mm) at 25°C. Strain amplitude (γ) sweep was conducted from γ= 0.01%-100% at frequency (ω) 1 rad/s.

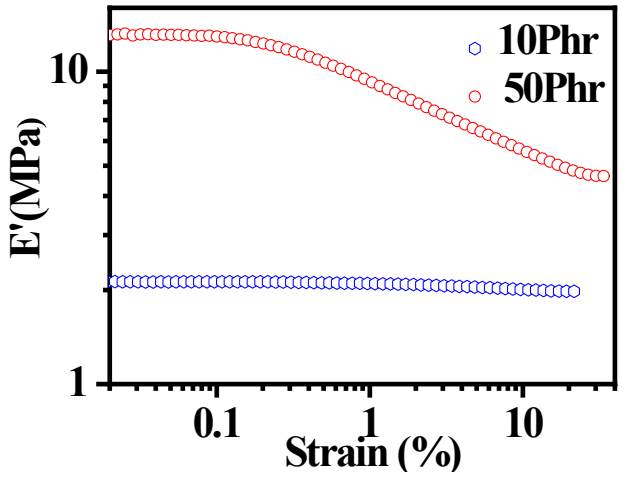

Figure S2. The measured Payne effects of CB10 and CB50

3. The Method for Filler Network Connectivity Determination

According to face-centered arrangement of effective inter-particle distance of adjacent CB aggregates as $d_c = (0.86\phi^{-1/3} - 1)d_{ave}$, where ϕ is CB volume fraction, d_{ave} is the average size of aggregates, CB aggregate with sizes larger than the effective inter-distance can be treated as the network in connection. A cut-off factor $\beta = \xi_i / d_c$ is defined to describe filler network connectivity, where aggregates with sizes (ξ_i) larger than d_c is considered as the network keeping connected. Then the percentage of filler network connectivity is expressed as $P_{net} = P_{//} \times P_{\perp}$. $P_{//(or\perp)} = N_{//(or\perp)}(\beta \geq 1) / N(\xi)$ is defined as filler network connectivity parallel or perpendicular to tensile direction and $N(\beta \geq 1)$ is the number of aggregates with sizes larger than d_c. With the size

distribution of aggregates obtained by X-ray imaging, the average connectivity of filler network under loading can be obtained.

4. The results of differences of CB volume resistivities in rubber matrix obtained by 3D-TEM and X-ray Nano-CT

To study the fine structures of CB filler in rubber matrix, including the single particles which not gathering to form aggregates, the 3D-TEM experiments were performed and the results were quantitatively analyzed. During 3D-TEM imaging, the rubber samples were cut into very thin pieces with thickness of ~70 nm. The quantitative volume resistivities of CB10 and CB50 are 4.9% and 18.9%, respectively, which are slightly larger than that obtained by X-ray Nano-CT (3.9% for CB10 and 17.5% for CB50, respectively). Because the spatial resolution of X-ray Nano-CT is also high (30 nm), only small part of single-particles may be lost in the experiment. The volume resistivities were averaged by three different pieces which were cut from different zones of one sample and the volume resistivity was 2.6%, 3.3% and 5.8% for CB10, and 15.4%, 17.7% and 19.5% for CB50, respectively. The results reflect the inhomogeneous distributions of CB filler in rubber matrix. Meanwhile, the CB aggregates were skeletonized and the average network connectivities (P_{net}) of CB10 and CB50 were 29.1% and 80.5%, respectively, which are slightly smaller than those obtained by X-ray Nano-CT (37.5% for CB10, and 95.7% for CB5, respectively). All these reflect the errors could be induced by the thin film in the experiments.

In all, both 3D-TEM and X-ray Nano-CT have their intrinsic advantages and

shortages: 3D-TEM owns higher spatial resolution (~1nm) but smaller field of view (several micrometers), while X-ray nano-CT has larger field of view (~50 μm) but smaller spatial resolution (~30nm). With respect to the network deformation investigated in current study, the X-ray nano-CT is preferred, which can provide more statistically reliable data. And the large open space in X-ray nano-CT provides sufficient space to track relatively large amount of rubber nano-composite even under loading conditions.

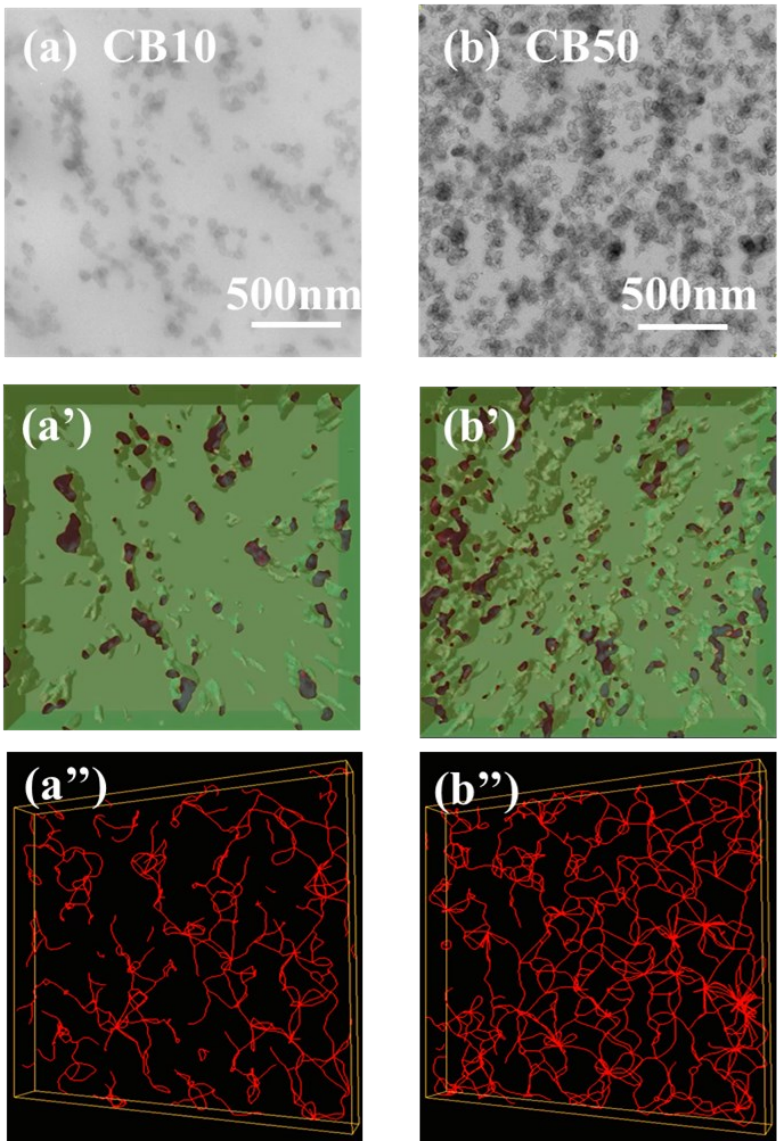

Figure S3: (a) The TEM projection, (a') 3D reconstruction and dying results and (a'')

The filler network structures of CB10. (b) The TEM projection, (b') 3D reconstruction and dying results and (b'') The filler network structures of CB50.

5. The 2D-WAXS Patterns of CB10 after Recovering for Different Times

For 2D-WAXS pattern measurement of CB10, the filled rubber films with dimensions of 10 mm × 5 mm × 1 mm were first fixed on a homemade tensile device, and stretched to the predetermined strains (ε=2.5) with the constant speed of 30 μm/s and kept for recovering with different time. Then the sample films were characterized with the tensile device installed in BL16B beamline in Shanghai Synchrotron Radiation Facility (SSRF) to follow SIC during second loading. *In-situ* WAXS measurements with X-ray wavelength of 0.124 nm and spot size of 1×2 mm^2 (X-ray energy: 10 keV) were conducted during the tensile stretch with a speed of 30 μm/s.

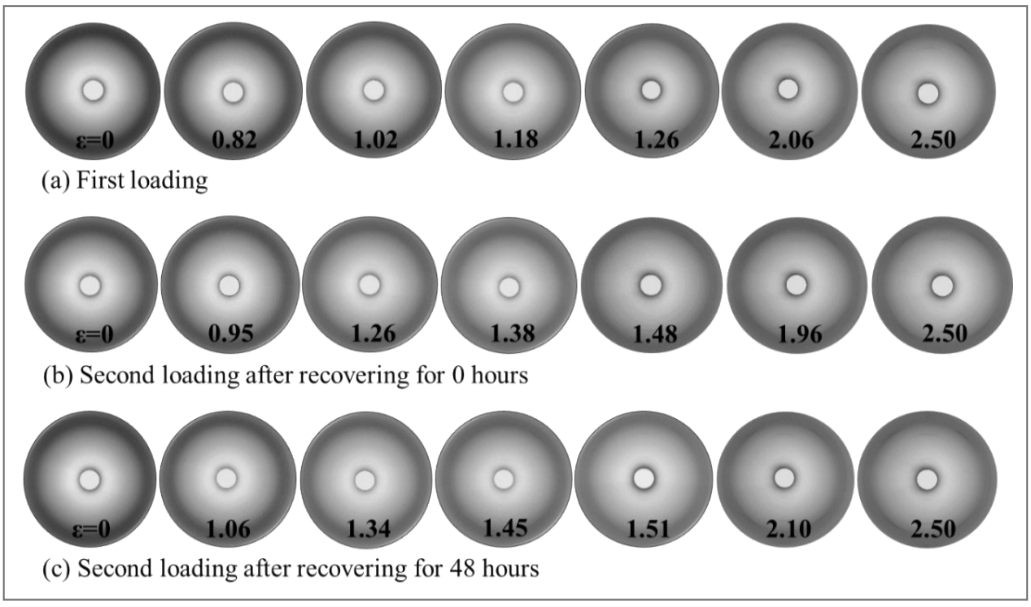

Figure S4: The 2D WAXS patterns of CB10 (a) in the first loading and (b) the second loading with a recovering time of 0 hr and (c) 48 hr. The deformation direction is horizontal.

4. WAXD Analysis

Following the described method, the patterns were masked with the FIT2D software to highlight the crystals. The different crystal planes ((200) and (201) planes) signal will be enlarged. Then the degree of crystallinities can be calculated with the areas of peak regions as: $C_{I200}\,(\%) = \frac{A_{200} + A_{120}}{A_{200} + A_{120} + A_{amor}} \times 100\%$ and $C_{I201}\,(\%) = \frac{A_{201}}{A_{201} + A_{amor}} \times 100\%$. Then $C_I = C_{I200} + C_{I201}$.

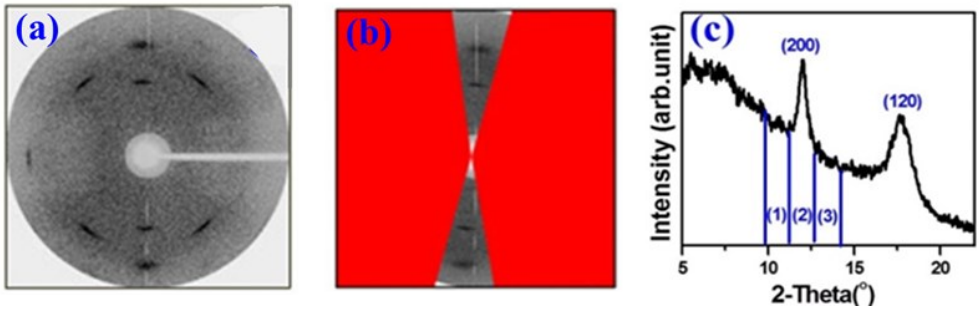

Figure S5. (a) A representative WAXS pattern at strain of 2.5; (b) The schematic illustrations for the (200) mask to the WAXS pattern in (a); (c) The 1D integrated profile for the WAXS pattern in (b).

5. Defect Fraction

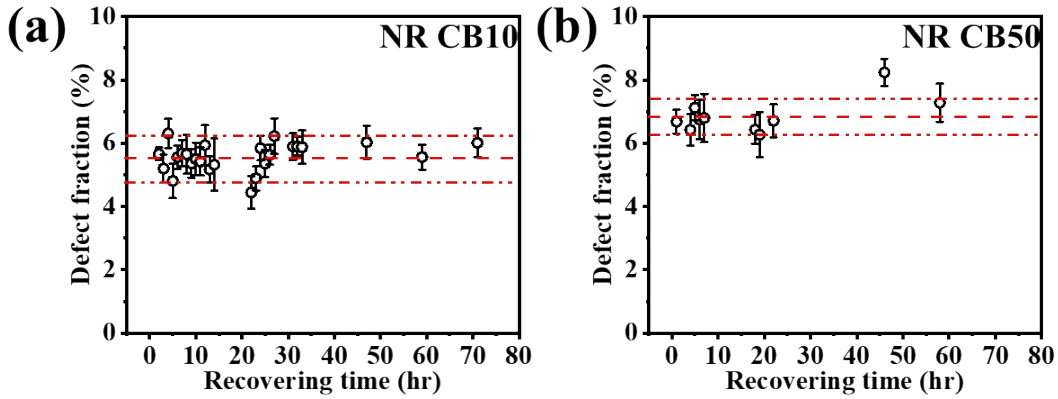

Figure S6. The defect fraction as a function of the recovering time of (a) CB10 and (b)

CB50.

6. Bound Rubber Fraction and Entangled Molecular Weight of Rubber Matrix of CB50 during Recovering

Following the same analysis procedure, the fraction of the bound rubber and the residual dipolar coupling strength for CB50 are summarized in Figure S7. Similar to the phenomenon of CB10, both parameters remain unchanged with increasing recovering time.

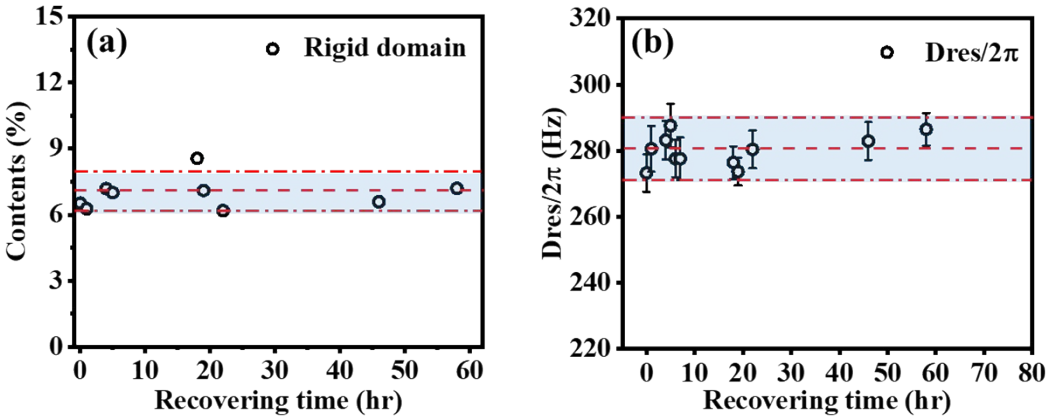

Figure S7. (a) The fraction of the bound rubber at different recovering time. (b) The residual dipolar coupling strength D_{res} as a function of the recovering time.

7. The absorption difference between carbon black and natural rubber with X-ray energies ranging from 280-1000 eV.

The densities of carbon black: 1.9 g/cm^3, natural rubber: 0.9 g/cm^3, respectively. Aggregate size: 300 nm.

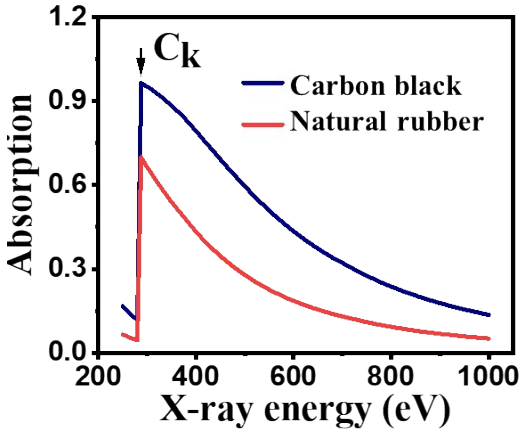

Figure S8: The absorption difference between carbon black and natural rubber